arXiv:1510.00901v2 [cond-mat.mes-hall] 6 Feb 2016

Tunneling Magnetoresistance in Junctions Composed of Ferromagnets and Time-Reversal Invariant Topological Superconductors

Zhongbo Yan[1,2,*] and Shaolong Wan[2]

[1]*Institute for Advanced Study, Tsinghua University, Beijing, 100084, China*
[2]*Department of Modern Physics, University of Science and Technology of China, Hefei, Anhui Province, 230026, China*

Tunneling Magnetoresistance between two ferrromagnets is an issue of fundamental importance in spintronics. In this work, we show that tunneling magnetoresistance can also emerge in junctions composed of ferromagnets and time-reversal invariant topological superconductors without spin-rotation symmetry. Here the physical origin is that when the spin-polarization direction of injected electron from the ferromagnet lying in the same plane of the spin-polarization direction of Majorana zero modes, the electron will undergo a perfect spin-equal Andreev reflection, while injected electrons with other spin-polarization direction will be partially Andreev reflected and partially normal reflected, which consequently have a lower conductance, and therefore, the magnetoresistance effect emerges. Compared to conventional magnetic tunnel junctions, an unprecedented advantage of the junctions studied here is that arbitrary high tunneling magnetoresistance can be obtained even the magnetization of the ferromagnets are weak and the insulating tunneling barriers are featureless. Our findings provide a new fascinating mechanism to obtain high tunneling magnetoresistance.

PACS numbers: 85.30.Mn, 85.75.-d, 03.65.Vf, 85.75.Dd

I. INTRODUCTION

Superconducting phase and ferromagnetic phase are two most familiar and classic symmetry-broken phases. The former one breaks the $U(1)$ gauge symmetry, while the latter one breaks the full spin-rotation symmetry (SRS) down to an axis-fixed rotation symmetry, as a consequence of symmetry breaking, the order parameter characterizing the superconductor (SC) takes a fixed phase, while the one characterizing the ferromagnet (FM) takes a fixed direction. Interestingly, the break down of the two symmetries has direct impact on the tunneling behavior of junctions composed of SCs or FMs. For junctions formed by two SCs sandwiching a thin insulator (also known as insulating tunneling barrier (ITB)) (SC-I-SC junction), the tunneling current depends on the phase-difference [1], while for junctions formed by two FMs sandwiching a thin insulator (FM-I-FM junction, known as magnetic tunnel junction (MTJ)), tunneling current depends on the angle-difference of the magnetization directions [2]. The former phenomenon is known as Josephson effect, while the latter one is known as magnetic valve effect (MVE) [3]. Both effects are very fascinating and have very wide applications, for the latter one, there is a quantity named as tunneling magnetoresistance (TMR) to characterize it. Higher TMR has always been pursed since the concept was proposed because a higher TMR implies a better performance of the effect in real applications, such as field sensor and magnetic random access memory [4–9].

SCs of nontrivial topological properties are known as topological superconductors (TSCs) [10]. Due to hosting the Majorana zero modes [11, 12] which have potential application in topological quantum computation [13, 14], TSC and topological superfluid (TSF) have been among the central themes of both condensed matter and cold atom physics in recent years [15–35]. According to the existence or absence of time-reversal symmetry, particle-hole symmetry and sublattice symmetry (or chiral symmetry), the TSCs can be classified in a ten-fold way [36–38]. It is interesting to find that TSCs in some classes, e.g. BDI class and DIII class, also break the SRS. Based on this observation, it leads us to expect that a FM-I-TSC junction will also exhibit TMR if the TSC breaks SRS. A direct investigation confirms our expectation and what interesting is that the nontrivial topological property of the SC endows nontrivial property to the TMR. For example, we find that for a generalized FM-I-FM-I-TSC junction, arbitrary high TMR can be obtained even the magnetization of the ferromagnets are weak and the insulating tunneling barriers are featureless.

The paper is organized as follows, in Sec.II, the theoretical model and main picture are given. In Sec.III and Sec.IV, the tunneling spectroscopies of a one-dimensional FM-I-TSC junction and a one-dimensional FM-I-FM-I-TSC junction are studied in detail, and based on the tunneling spectroscopies, TMR's dependence on parameters are obtained. In Sec.V, the higher dimensional case of the FM-I-FM-I-TSC junction is studied, and similar results like the one-dimensional case are obtained. In Sec.VI, discussions and conclusions about the results obtained in previous sections are given.

II. THE THEORETICAL MODEL AND MAIN PICTURE

The general picture of the junction structure we will study is illustrated in Fig.1(a). But to obtain a clear physical picture, we will first study the simplest case, a one-dimensional FM-I-TSC junction. Before we write down the Hamiltonian, it is worth stressing the fact that in one dimension, if the Cooper pairs of the superconductor is spin-polarized ($S_z \neq 0$, $\vec{S}$ is the total spin angular momentum of the Cooper pair), the zero-bias conductance (ZBC) of a FM-I-TSC is always quan-

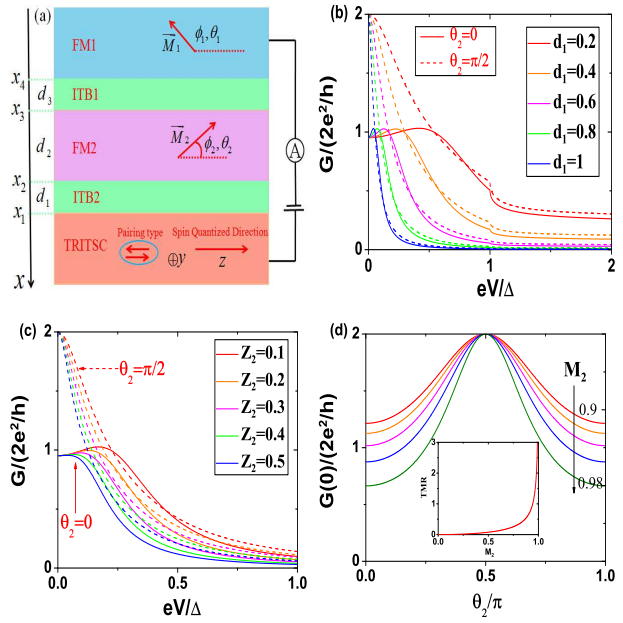

FIG. 1. Sketch of the system and tunneling spectroscopy of FM-I-TS junction. (a) The spin quantization axis of the time-reversal invariant TSC (TRITSC) is chosen along the z direction, the magnetization direction of FM1 and FM2 are characterized by (ϕ_1, θ_1) and (ϕ_2, θ_2), respectively. Common parameters in (b)(c)(d), $\mu_f = \mu_I = \mu_s = 1$ (μ_f is taken as the energy unit), $\Delta_0 = 0.01$, other parameters: (b) $M_2 = 0.95$, $Z_1 = Z_2 = 0.1$, Δ is the energy gap of the TSC. (c) $M_2 = 0.95$, $d_1 = 0.5$, $Z_1 = 0.1$. (d) The dependence of ZBC on θ_2 and magnetization strength, the inset shows the TMR's dependence on magnetization strength.

tized no matter what magnetization direction the FM chooses. Therefore, to obtain remarkable TMR, the TSC needs to be time-reversal invariant and the Cooper pairs need to be un-spin-polarized ($S_z = 0$) [39–42].

Although we plan to study the one-dimensional FM-I-TSC junction firstly, here for compactness, we will write down the general Hamiltonian describing the system illustrated in Fig.1(a). Under the representation $\hat{\Psi}^\dagger(x) = (\hat{\psi}^\dagger_\uparrow(x), \hat{\psi}_\downarrow(x), \hat{\psi}^\dagger_\downarrow(x), \hat{\psi}_\uparrow(x))$, the general one-dimensional (higher dimensions will be studied in lateral section) Hamiltonian is given as ($\hbar = m = 1$) [43]

$$\mathcal{H} = \tau_z \left[-\frac{\partial_x^2}{2} - \mu(x) + V(x) \right] + \tau_x \Delta(x), \tag{1}$$

where $\vec{\tau} = (\tau_x, \tau_y, \tau_z)$ are Pauli matrices in particle-hole space, $V(x)$ is potential induced by disorder, external field, etc, here we assume it takes the form

$$V(x) = -\tau_z M_1(\vec{n}_1 \cdot \vec{\sigma})\Theta(x_3 - x) - \tau_z M_2(\vec{n_2} \cdot \vec{\sigma}) \Theta(x - x_2)\Theta(x_1 - x) + \sum_{i=1}^{4} Z_i \delta(x_i - x), \tag{2}$$

the terms in the first line denote the magnetization of FM1 and FM2, M_1 and M_2 denote the magnetization strength of FM1 and FM2, while $\vec{n}_1 = (\cos\phi_1 \sin\theta_1, \sin\phi_1 \sin\theta_1, \cos\theta_1)$ and $\vec{n}_2 = (\cos\phi_2 \sin\theta_2, \sin\phi_2 \sin\theta_2, \cos\theta_2)$ denote the magnetization directions of FM1 and FM2, respectively; $\sigma_{x,y,z}$ are Pauli matrices acting on the spin space, $\Theta(x)$ is the Heaviside function, $i.e.$, $\Theta(x > 0) = 1$, $\Theta(x < 0) = 0$; the terms in the second line denote the scattering potential at the interfaces; $\mu(x)$ is the chemical potential, we set $\mu(x) = \mu_f$ (or E_F) for the two FMs, $\mu(x) = -\mu_I$ for the two insulating tunneling regions, and $\mu(x) = \mu_s > 0$ for the SC. $\Delta(x) = -i\Delta_0\Theta(x - x_1)\partial_x$ is the pairing potential, which is assumed to be p-wave type (then as $\mu_s > 0$ is assumed, the SC is a TSC with Majorana zero modes located at the boundary [44, 45]) and homogeneous at $x > x_1$ and vanish at $x < x_1$ for the sake of theoretical simplicity.

To see that the TSC breaks the SRS, we transform the Hamiltonian corresponding to the superconducting part into momentum space, then under the representation $\hat{\Psi}^\dagger(k) = (\hat{\psi}^\dagger_\uparrow(k), \hat{\psi}_\downarrow(-k), \hat{\psi}^\dagger_\downarrow(k), \hat{\psi}_\uparrow(-k))$

$$\mathcal{H}_{sc}(k) = [\frac{k^2}{2} - \mu_s]\tau_z\sigma_0 + \Delta(k)\tau_x\sigma_0. \tag{3}$$

where $\Delta(k) = \Delta_0 k$, σ_0 is the 2×2 unit matrix in spin space. By making a spin-rotation: $\hat{\psi}_\uparrow(k) \to \cos\theta\hat{\psi}_\uparrow(k) + \sin\theta\hat{\psi}_\downarrow(k)$, $\hat{\psi}_\downarrow(k) \to -\sin\theta\hat{\psi}_\uparrow(k) + \cos\theta\hat{\psi}_\downarrow(k)$, it is easy to check that the superconducting term, $\Delta_0 k\hat{\psi}^\dagger_\uparrow(k)\hat{\psi}^\dagger_\downarrow(-k) + h.c.$, is not invariant, and therefore breaks the SRS. The time-reversal symmetry of the Hamiltonian is easy to check: $\mathcal{T}\mathcal{H}_{sc}(k)\mathcal{T}^{-1} = \mathcal{H}_{sc}(-k)$ with $\mathcal{T} = \tau_z K$, where K is the complex conjugate operator.

To obtain the tunneling spectroscopies of the junction, here we follow the Slonczewski [3] and Blonder-Tinkham-Klapwijk (BTK) approach [46–48]. The first step of the approach is to write down the wave functions of each part of the junctions. If we consider that a majority electron with energy E (relative to μ_f) is injected from FM1, the wave function in FM1 is given as

$$\psi_{FM1} = \vec{\chi}_1 e^{ik_{1+,e}x} + b_{1+}\vec{\chi}_1 e^{-ik_{1+,e}x} + a_{1+}\vec{\chi}_2 e^{ik_{1+,h}x} + b_{1-}\vec{\chi}_3 e^{-ik_{1-,e}x} + a_{1-}\vec{\chi}_4 e^{ik_{1-,h}x} \tag{4}$$

with

$$\vec{\chi}_1 = (\eta_1, 0, \eta_2 e^{i\phi_1}, 0)^T, \vec{\chi}_2 = (0, \eta_2, 0, \eta_1 e^{i\phi_1})^T, \vec{\chi}_3 = (-\eta_2, 0, \eta_1 e^{i\phi_1}, 0)^T, \vec{\chi}_4 = (0, -\eta_1, 0, \eta_2 e^{i\phi_1})^T, \tag{5}$$

where $\eta_1 = \cos(\theta_1/2)$, $\eta_2 = \sin(\theta_1/2)$ and $k_{1+,e(h)} = \sqrt{2(\mu_f + M_1 + (-)E)}$, $k_{1-,e(h)} = \sqrt{2(\mu_f - M_1 + (-)E)}$. The coefficients $b_{1+(-)}$ and $a_{1+(-)}$ denote the spin-equal (spin-opposite) normal reflection (a majority electron reflected as a majority (minority) electron) amplitude and spin-equal (spin-opposite) Andreev reflection (a majority electron reflected as a majority (minority) hole [49]) amplitude, respectively. The wave functions in other parts can be obtained easily but as their forms are tedious, their concrete expressions will be given in the Appendix.

To obtain the tunneling conductance, the coefficients in the wave functions need to be determined by matching the wave

functions at the interfaces according to the boundary conditions [3, 46–48]

$$\psi_L(x=x_i)=\psi_R(x=x_i),$$
$$v_{i,R}\psi_R(x_i^+)-v_{i,L}\psi_L(x_i^-)=-i2Z_i\tau_z\sigma_0\psi_R(x_i), \quad (6)$$

where $\psi_L(x=x_i)$ ($\psi_R(x=x_i)$) denotes the wave function in the left (right) neighbouring part of the interface located at $x=x_i$, $v_{i,R(L)}=\partial\mathcal{H}_{i,R(L)}/\partial k$ is the velocity operator corresponding to the right (left) neighboring part of the interface [44].

After the coefficients are obtained, the zero temperature tunneling conductance can be determined according to the BTK formula [46]

$$G_+(E=eV,\vec{n}_1,\vec{n}_2)=\frac{e^2}{h}(1+A_+ +A_- -B_+ -B_-) \quad (7)$$

where $A_+ = k_{1+,h}|a_{n+}|^2/k_{1+,e}$, $B_+ = |b_{1+}|^2$, $A_- = k_{1-,h}|a_{1-}|^2/k_{1+,e}$, $B_- = k_{1-,e}|b_{1-}|^2/k_{1+,e}$. Similar procedures can obtain $G_-(eV,\vec{n}_1,\vec{n}_2)$, the tunneling conductance for a minority electron, and the total tunneling conductance $G(eV,\vec{n}_1,\vec{n}_2)$ is given as the summation of $G_+(eV,\vec{n}_1,\vec{n}_2)$ and $G_-(eV,\vec{n}_1,\vec{n}_2)$.

III. ONE-DIMENSIONAL FM-I-TSC JUNCTION

Now, we are going to study the one-dimensional FM-I-TSC junction. For the FM-I-TSC junction, we consider that it is only composed of FM2, ITB2 and TSC, and x_3 is set to infinity. For this structure, the wave function in FM2 takes the same form as ψ_{FM1}, but with a substitution of the parameters: $(k_{1+(-),e(h)},\theta_1,\phi_1)\to(k_{2+(-),e(h)},\theta_2,\phi_2)$, where $k_{2+,e(h)}=\sqrt{2(\mu_f+M_2+(-)E)}$, $k_{2-,e(h)}=\sqrt{2(\mu_f-M_2+(-)E)}$.

By a simple numeric calculation of the coefficients of the wave functions, the tunneling conductance of the FM-I-TSC junction is shown in Fig.1(b)(c). There are two extraordinary characteristics in the tunneling spectroscopy. The first one is that the tunneling conductance is angle-dependent, the second one is that the tunneling conductance at zero-bias voltage is of topological feature in the sense that it is independent of the thickness of ITB2 and the interface scattering potential. In fact, at zero-bias voltage, the four key quantities A_+, A_-, B_+ and A_- can be analytically obtained. When we consider that a majority electron is injected, their analytical forms are

$$A_+=\frac{16k_{2+}^2k_{2-}^2\sin^2\theta_2}{[(k_{2+}+k_{2-})^2\cos^2\theta_2+4k_{2+}k_{2-}\sin^2\theta_2]^2},$$
$$A_-=\frac{4k_{2+}k_{2-}(k_{2+}+k_{2-})^2\cos^2\theta_2}{[(k_{2+}+k_{2-})^2\cos^2\theta_2+4k_{2+}k_{2-}\sin^2\theta_2]^2},$$
$$B_+=\frac{(k_{2+}^2-k_{2-}^2)^2\cos^4\theta_2}{[(k_{2+}+k_{2-})^2\cos^2\theta_2+4k_{2+}k_{2-}\sin^2\theta_2]^2},$$
$$B_-=\frac{4k_{2+}k_{2-}(k_{2+}-k_{2-})^2\sin^2\theta_2\cos^2\theta_2}{[(k_{2+}+k_{2-})^2\cos^2\theta_2+4k_{2+}k_{2-}\sin^2\theta_2]^2}, \quad (8)$$

where $k_{2+(-)}=\sqrt{2(\mu_f+(-)M_2)}$. If a minority electron is injected, the four key quantities have such an exchange, $A_+\leftrightarrow A_-$, $B_+\leftrightarrow B_-$. Then according to the eq.(7), it is direct to obtain

$$G(0,\vec{n}_2)=\frac{e^2}{h}\frac{16k_{2+}k_{2-}}{(k_{2+}+k_{2-})^2\cos^2\theta_2+4k_{2+}k_{2-}\sin^2\theta_2} \quad (9)$$

The zero-bias conductance (ZBC) only depends on θ_2 and the parameters of FM2. From the formula we can see that $G(0,\vec{n}_2)$ is quantized as $4e^2/h$ at $\theta_2=\pi/2$ and takes its minimum value at $\theta_2=0$ and $\theta_2=\pi$, as shown in fig.1(d). In a recent work [43], we have proven that by making use of this minimum value, it is very convenient to determine the polarization of FMs. From eq.(8) or more directly from fig.2(a)(b), we can see that at $\theta_2=\pi/2$, $A_+=1$, while the other three quantities are all equal to zero, which indicates a perfect spin-equal Andreev reflection. As this perfect spin-equal Andreev reflection is unaffected by the ITB2 and the scattering potential, here the only possible origin is the resonant tunneling due to the topological Majorana zero modes located at the boundary of the TSC. In ref.[50], by using scattering matrix, the authors have shown that perfect spin-equal Andreev reflection will occur when the injected electron takes certain spin-polarization direction. In the following, we will show that here the magic direction is just the spin-polarization direction of the Majorana zero modes.

To obtain the zero modes in the TSC, we need to calculate the BdG equation, which is given as

$$Eu_\uparrow(x)=(-\frac{\partial_x^2}{2}-\mu)u_\uparrow(x)-i\Delta\partial_x v_\downarrow(x),$$
$$Ev_\downarrow(x)=-i\Delta\partial_x u_\uparrow(x)+(\frac{\partial_x^2}{2}+\mu)v_\downarrow(x),$$
$$Eu_\downarrow(x)=(-\frac{\partial_x^2}{2}-\mu)u_\downarrow(x)-i\Delta\partial_x v_\uparrow(x),$$
$$Ev_\uparrow(x)=-i\Delta\partial_x u_\downarrow(x)+(\frac{\partial_x^2}{2}+\mu)v_\uparrow(x), \quad (10)$$

with the boundary condition that the wave functions $u_\uparrow(x)$, $v_\downarrow(x)$, $u_\downarrow(x)$ and $v_\uparrow(x)$ all need to vanish at $x=0$ and $x=+\infty$. For the zero modes, $i.e.$, $E=0$, a direct calculation gives

$$u_\uparrow(x)=iv_\downarrow(x)=\mathcal{N}\sin(\kappa x)e^{-\gamma x},$$
$$u_\downarrow(x)=iv_\uparrow(x)=\mathcal{N}\sin(\kappa x)e^{-\gamma x}, \quad (11)$$

where $\kappa=\sqrt{2\mu-\Delta^2}$, $\gamma=\Delta$, and $\mathcal{N}$ is the normalization constant which guarantees $\int_0^{+\infty}dx(|u_{,\uparrow(\downarrow)}(x)|^2+|v_{\downarrow(\uparrow)}(x)|^2)=1$, then the zero modes located at the $x=0$ boundary is given as

$$C_1=|\mathcal{N}|\int dx[e^{\frac{i\pi}{4}}\psi_\uparrow(x)+e^{-\frac{i\pi}{4}}\psi_\downarrow^\dagger(x)]\sin(\kappa x)e^{-\gamma x},$$
$$C_2=|\mathcal{N}|\int dx[e^{\frac{i\pi}{4}}\psi_\downarrow(x)+e^{-\frac{i\pi}{4}}\psi_\uparrow^\dagger(x)]\sin(\kappa x)e^{-\gamma x}, \quad (12)$$

here we have chosen $\mathcal{N}=|\mathcal{N}|e^{i\pi/4}$ for the convenience of the following discussions. By using the normalization condition, it is direct to verify $\{C_1,C_1^\dagger\}=\{C_2,C_2^\dagger\}=1$. It is

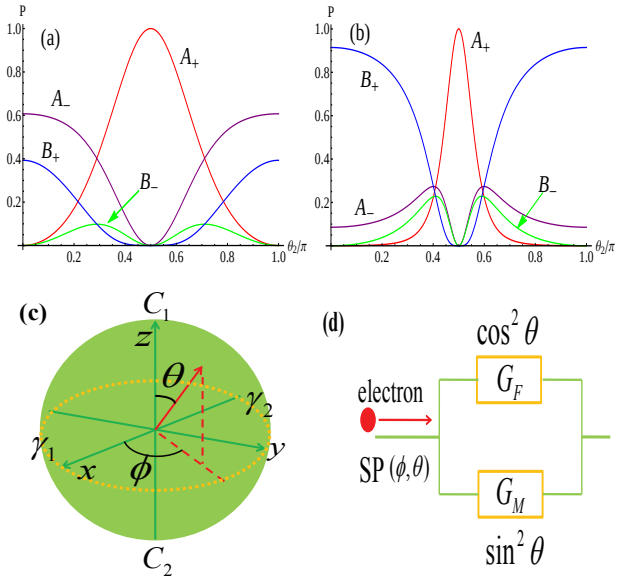

FIG. 2. The four reflection coefficients with (a) $M_2/\mu_f = 0.9$ and (b) $M_2/\mu_f = 0.9999$. (c) Spin-polarization direction of the zero modes. (d) A circuit picture to understand the tunneling process and the result given in eq.(9).

also easy to see that C_1 and C_2 are related with each other by the charge conjugate, *i.e.*, $C_1^\dagger = C_2$, but $C_1^\dagger \neq C_1$ and $C_2^\dagger \neq C_2$, this indicates that the two fermionic zero modes C_1 and C_2 are not of Majorana characteristic. However, from the Kitaev Majorana chain model we already know that a fermion operator with its conjugate can construct two Majorana operators [11], here as $C_1^\dagger = C_2$, the two Majorana zero modes can be constructed as

$$\gamma_1 = \frac{C_1 + C_1^\dagger}{\sqrt{2}}, \gamma_2 = \frac{C_1 - C_1^\dagger}{\sqrt{2}i}, \tag{13}$$

the Majorana zero modes are an equal-weight superposition of the two fermionic zero modes.

Based on eq.(12) and eq.(13), the spin-polarization of the zero modes can be directly calculated,

$$\begin{aligned}
&< C_1|\hat{S}_x|C_1 > = < C_1|\hat{S}_y|C_1 >= 0, < C_1|\hat{S}_z|C_1 >= \frac{\hbar}{2},\\
&< C_2|\hat{S}_x|C_2 > = < C_2|\hat{S}_y|C_2 >= 0, < C_2|\hat{S}_z|C_2 >= -\frac{\hbar}{2},\\
&< \gamma_1|\hat{S}_y|\gamma_1 > = < \gamma_1|\hat{S}_z|\gamma_1 >= 0, < \gamma_1|\hat{S}_x|\gamma_1 >= \frac{\hbar}{2},\\
&< \gamma_2|\hat{S}_y|\gamma_2 > = < \gamma_2|\hat{S}_z|\gamma_2 >= 0, < \gamma_2|\hat{S}_x|\gamma_2 >= -\frac{\hbar}{2},
\end{aligned} \tag{14}$$

where $|C_1 >= (e^{-\frac{i\pi}{4}}(i\psi_\uparrow + \psi_\downarrow^\dagger))^\dagger|0>$, $|C_2 >= (e^{-\frac{i\pi}{4}}(i\psi_\downarrow + \psi_\uparrow^\dagger))^\dagger|0>$, $|\gamma_1 >= (e^{-\frac{i\pi}{4}}/\sqrt{2})(i\psi_\uparrow + \psi_\downarrow^\dagger + i\psi_\downarrow + \psi_\uparrow^\dagger)|0>$, $|\gamma_1 >= (e^{-\frac{i\pi}{4}}/\sqrt{2}i)(i\psi_\uparrow + \psi_\downarrow^\dagger - i\psi_\downarrow - \psi_\uparrow^\dagger)|0>$, and $\hat{S}_x = \frac{\hbar}{2}(\psi_\uparrow^\dagger\psi_\downarrow + \psi_\downarrow^\dagger\psi_\uparrow)$, $\hat{S}_y = \frac{-i\hbar}{2}(\psi_\uparrow^\dagger\psi_\downarrow - \psi_\downarrow^\dagger\psi_\uparrow)$, $\hat{S}_z = \frac{\hbar}{2}(\psi_\uparrow^\dagger\psi_\uparrow - \psi_\downarrow^\dagger\psi_\downarrow)$. From eq.(14), it is direct to see that the spin-polarization directions of the two fermionic zero modes C_1 and C_2 are along the positive z-direction and negative z-direction, respectively, while the spin-polarization of the two Majorana zero modes γ_1 and γ_2 are along the positive x-direction and negative x-direction, respectively, which is a natural result according to eq.(13). Projecting the spin-polarization on the Bloch sphere, the spin-polarization directions of the two fermionic zero modes C_1 and C_2 point to the north pole ($\theta_2 = 0$) and south pole ($\theta_2 = \pi$), respectively, while the spin-polarization directions of the two Majorana zero modes are lying in the equatorial plane, which corresponds to $\theta_2 = \pi/2$, as shown in fig.2(c).

Based on these results, the physical picture is clear: when the spin-polarization direction of the injected electron is along the z-direction, $\theta_2 = 0$ or $\theta_2 = \pi$, the injected electron only feels one of the fermionic zero modes and the only possible Andreev reflection is the spin-opposite Andreev reflection. For the spin-opposite Andreev reflection, the Fermi-surface mismatch in the FM due to the magnetization will suppress it and therefore, it can not be perfect and spin-equal normal reflection will take place, as shown in fig.2(a)(b). But as the fermionic zero modes are of topological nature, the insulating tunneling barrier and the interface scattering potential can not affect the spin-opposite Andreev reflection. When the spin-polarization direction of the injected electron is lying in the equatorial plane, *i.e.*, $\theta_2 = \pi/2$, it feels the two fermionic zero modes equally and is equivalent to couple with the Majorana zero modes, and then the only possible Andreev reflection is the spin-equal Andreev reflection (because the electron coupled with either one of the two Majorana zero modes will undergo a perfect spin-equal Andreev reflection, the azimuthal angle ϕ_2 has no effect to the tunneling process). For the spin-equal Andreev reflection, however, the magnetization has no effect to it and therefore, the electron will undergo a perfect Andreev reflection and consequently results in a quantized conductance. For the general case that the spin-polarization direction of the injected electrons is neither along the fermionic zero modes' nor the majorana zero modes', the electron can be divided into two parts, one along the spin-polarization direction of the fermionic zero modes and the other one along the Majorana zero modes'. Based on this division, the conductance given in eq.(9) can also correspondingly be divided into two parts,

$$\frac{1}{G(0,\vec{n}_2)} = \frac{1}{G_F}\cos^2\theta_2 + \frac{1}{G_M}\sin^2\theta_2, \tag{15}$$

where $G_F = 16k_{2+}k_{2-}G_0/(k_{2+}+k_{2-})^2$ and $G_M = 4G_0$ with $G_0 = e^2/h$, G_F corresponds to the process that the injected electron is coupled with only one of the fermionic zero modes, and G_M corresponds to the process that the injected electron is coupled with the Majorana zero modes. The physical meaning of eq.(15) is that the two processes form a parallel circuit as shown in fig.2(d). An even more clear picture can be obtained if the conductance is substituted by resistance, *i.e.*, $R = 1/G$, then eq.(15) is correspondingly rewritten as

$$R(0,\vec{n}_2) = R_F\cos^2\theta_2 + R_M\sin^2\theta_2. \tag{16}$$

The physical meaning of eq.(16) is that the total resistance of the tunneling process is a sum of the resistances of the two possible tunneling processes, which is obviously physical right.

As $G(0,\vec{n}_2)$ has an explicit angle dependence, the junction will naturally exhibit TMR. Because low-bias voltage corresponds to low-energy consumption which is very important for real applications, the low-bias regime is of central interest. Therefore, in the following, when we consider the TMR, we will restrict ourselves to the zero-bias voltage. In the low-bias regime, $eV << \Delta$, where Δ is the energy gap of TSC, the effect of increasing the bias voltage is a reduction of the TMR, but the reduction will be quite limited and the main physics obtained at zero-bias voltage will still hold.

Generally, TMR is defined as

$$\mathrm{TMR} = \frac{R_{\mathrm{ap}} - R_{\mathrm{p}}}{R_{\mathrm{p}}} = \frac{R_{\mathrm{max}} - R_{\mathrm{min}}}{R_{\mathrm{min}}}, \tag{17}$$

where R_{ap} is the electrical resistance in the anti-parallel state, whereas R_{p} is the resistance in the parallel state. However, here a better definition is given as

$$\mathrm{TMR} = \frac{G_{\mathrm{max}} - G_{\mathrm{min}}}{G_{\mathrm{min}}}, \tag{18}$$

According to the formula (18) and (9), the TMR of the junction is given as

$$\mathrm{TMR} = \frac{(k_{2+} - k_{2-})^2}{4k_{2+}k_{2-}}. \tag{19}$$

Since the ZBC is of topological feature, here the TMR is also of topological feature, which is fundamentally different from the usual cases [3].

In eq.(19), with the increase of magnetization strength, k_{2-} will continue to decrease to zero, and then TMR will go to diverge, as shown in the inset of fig.1(d). The divergent behavior indicates that if the FM turns to be a half metal, the MVE is perfect even there is only one FM. However, as shown in fig.1(d), the increase of TMR is quite slow, even when M_2/μ_f reaches 90%, the TMR is still smaller than 100%, this implies that only when the FM is close to perfect polarization, a very high TMR can be obtained. The request of strong magnetization will greatly limit the applicable ferromagnetic materials and consequently reduces the novelty of the new MVE. In the following section, we will show that a generalized FM-I-FM-I-TSC junction overcomes this shortcoming.

IV. ONE-DIMENSIONAL FM-I-FM-I-TSC JUNCTION

The tunneling spectroscopies of the one-dimensional FM-I-FM-I-TSC junction are shown in fig.3 and fig.4, the most remarkable property of the tunneling spectroscopies is that when $\theta_2 = \pi/2$, the ZBC keeps the topological feature (as shown in fig.3(a)(b)) and is found to take the same form as

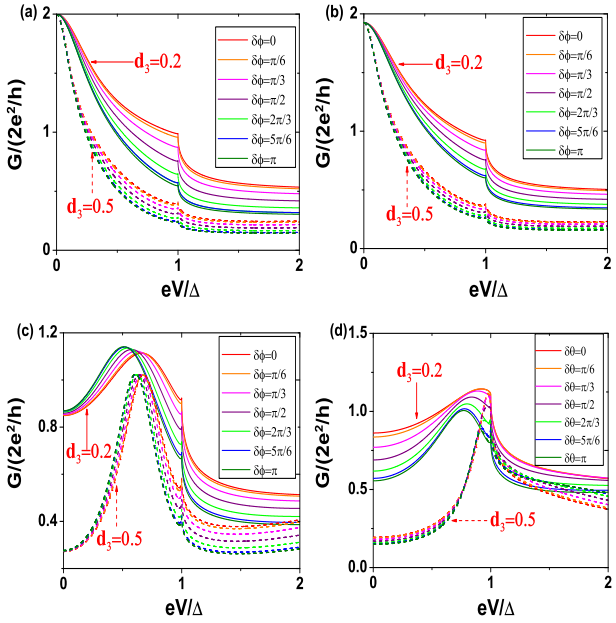

FIG. 3. Tunneling spectroscopy of FM-I-FM-I-TS junction and tunneling conductance's dependence on the magnetization directions of FMs. Common parameters in all figures, $\mu_f = \mu_I = \mu_s = 1$, $\Delta_0 = 0.05$, $M_1 = M_2 = 0.5$, $d_1 = 0.2$, d_2=1, $Z_{1,2,3,4} = 0.1$. Tunneling spectroscopy with (a) $\theta_1 = \theta_2 = \pi/2$, (b) $\theta_1 = 0$, $\theta_2 = \pi/2$, (c) $\theta_1 = 3\pi/4$, $\theta_2 = \pi/4$, (d) $\delta\phi = \phi_1 - \phi_2 = 0$, $\theta_2 = 0$. The conductance only depends on the difference of ϕ_1 and ϕ_2, does not depend on the absolute value of ϕ_1 and ϕ_2.

eq.(9) but with a substitution of $(k_{2+(-)}, \theta_2)$ to $(k_{1+(-)}, \theta_1)$, *i.e.*,

$$\tilde{G}(0,\vec{n}_1,\theta_2 = \frac{\pi}{2}) = \frac{e^2}{h}\frac{16k_{1+}k_{1-}}{(k_{1+}+k_{1-})^2\cos^2\theta_1 + 4k_{1+}k_{1-}\sin^2\theta_1}$$

with $k_{1+(-)} = \sqrt{2(\mu_f + (-)M_1)}$. It is interesting that $\tilde{G}(0,\vec{n}_1,\theta_2 = \pi/2)$ is independent of the magnetization strength of FM2 but only depends on the parameters of FM1, this is a manifestation of the non-local effect of the nontrivial topology of TSC. When $\theta_2 \neq \pi/2$, the ZBC no longer exhibits the topological feature and turns to depend on all parameters of the whole junction.

In fig.3(a), $\theta_1 = \theta_2 = \pi/2$, *i.e.*, $\delta\theta = \theta_1 - \theta_2 = 0$, by varying $\delta\phi = \phi_1 - \phi_2$, it is found that the tunneling conductance away from the zero-bias voltage shows the conventional MVE between two FMs since the conductance in the parallel state is larger than the one in the anti-parallel state. Similar picture also appears when $\delta\phi$ is fixed to zero while varying $\delta\theta$ with θ_2 fixed, as shown in fig.3(d). However, the results shown in fig.3(b)(c) can not be explained by the MVE between two FMs because the angle-difference between the two magnetization direction is fixed to $\pi/2$ (the angle difference is given as $\arccos(\cos(\delta\theta)\cos(\delta\phi))$, as $\delta\theta = \pi/2$, the varying of the $\delta\phi$ does not change the angle-difference), this suggests that the appearance of TSC enriches the angle-dependence. From these figures, it is also direct to see that when $\theta_2 \neq \pi/2$,

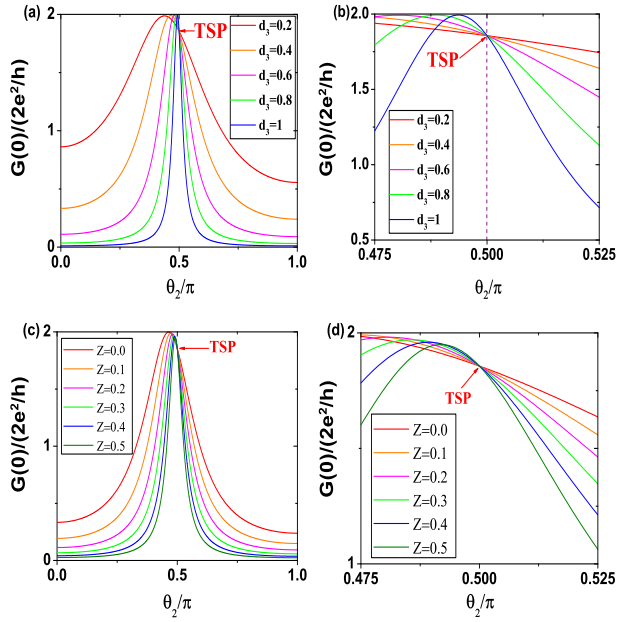

FIG. 4. ZBC's dependence on the thickness of ITB1 and interface scattering potential. Common parameters in all figures, $\mu_f = \mu_I = \mu_s = 1$, $\Delta_0 = 0.05$, $M_1 = M_2 = 0.5$, $d_2 = 1$, $\theta_1 = \phi_1 = \phi_2 = 0$. (a)-(b) $Z_{1,2,3,4} = 0.1$, $d_1 = 0.2$, (a) shows the dependence of ZBC on the thickness of ITB1, d_3, (b) shows a closer look of the topological stable point (TSP) in (a). (c)-(d) $d_1 = d_3 = 0.5$, $Z_{1,2,3,4} = Z$. (c) shows the dependence of ZBC on interface scattering potential, Z, (d) shows a closer look of the TSP in (c).

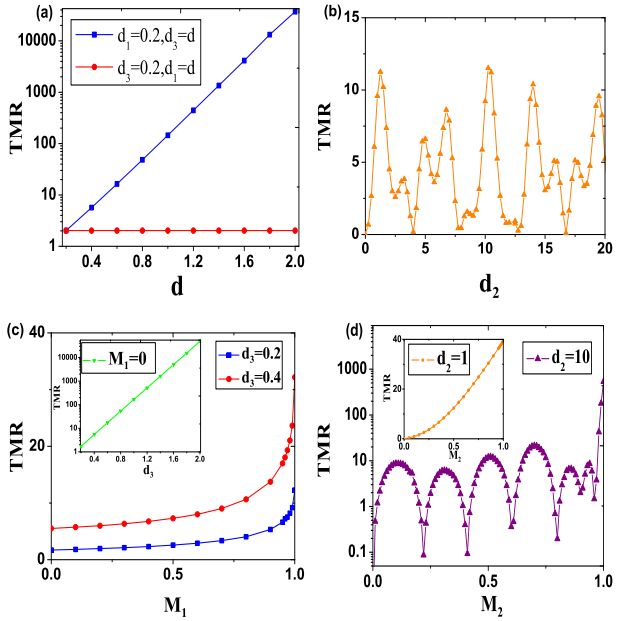

FIG. 5. TMR's dependence on parameters of FM-I-FM-I-TS junction. Common parameters in all figures, $\mu_f = \mu_I = \mu_s = 1$, $\Delta_0 = 0.05$, $\theta_1 = \phi_1 = \phi_2 = 0$. (a) TMR's dependence on the thickness of ITB, $M_1 = M_2 = 0.5$, $d_2 = 1$. (b) TMR's dependence on the length of FM2, $M_1 = M_2 = 0.5$, $d_1 = d_3 = 0.5$. (c) TMR's dependence on the magnetization strength of FM1, $M_2 = 0.5$, $d_1 = 0.2$, $d_2 = 1$. (d) TMR's dependence on the magnetization strength of FM2, $M_1 = 0.5$, $d_1 = d_3 = 0.5$. In (a)(d), logarithmic coordinates are used.

the increase of the thickness of the ITB1, d_3, will greatly reduce the conductance's dependence on the angle-difference between the two FMs. As we will show in the following that the TMR grows exponentially with d_3, this indicates that the TMR's dependence on the angle-difference between the two FMs can be safely neglected in the high TMR regime which is of most interest. Based on this recognition, without loss of the main physics, we set $\theta_1 = \phi_1 = \phi_2 = 0$, while keeping θ_2 as the only variable.

In fig.3(c)(d), it has already shown that with the increase of d_3, the tunneling conductance at low-bias voltage will be greatly suppressed. Fig.4(a) provides a more complete picture of the ZBC's dependence on θ_2 and the effect of d_3 to the ZBC. It is clear that the minimum ZBC decreases monotonically with d_3, but for the ZBC at $\theta_2 = \pi/2$, the increase of d_3 has no effect to it, as shown in Fig.4(b). From the expression of $\tilde{G}(0, \vec{n}_1, \theta_2 = \pi/2)$ we know it takes the value $16k_{1+}k_{1-}G_0/(k_{1+} + k_{1-})^2$. Fig.4(c)(d) show the effect of the interface scattering potential to the ZBC, it is easy to see that the results are similar to fig.4(a)(b).

Since the increase of d_3 and the increase of interface scattering potential both have no effect to the ZBC at $\theta_2 = \pi/2$, but will greatly suppress the ZBC away from $\theta_2 = \pi/2$, it is obvious that the increase of d_3 and the increase of interface scattering potential will greatly increase the TMR. In fig.5(a), the blue square-line shows that the TMR grows exponentially with the increase of d_3. This is a remarkable property, because it indicates that the TMR is easy to tune and can be tuned to arbitrary high value even the two FMs are both weak. Unlike the conventional MVE between two FMs that the increase of the thickness of ITB will exponentially suppress the tunneling conductance (or say tunneling current) for all possible angle-difference, here due to the nontrivial topological property of the TSC, the tunneling conductance at the neighbourhood of $\theta_2 = \pi/2$ is topologically stable and therefore, even d_3 is large, the tunneling current can still be large. This is also important for real applications because the strength of the tunneling current is proportional to the strength of signal, therefore a high signal-to-noise ratio, which is necessary for storage applications [7], can be guaranteed in this system. The TMR's explicit dependence on the interface scattering potential of each interface is neglected here, the only thing we need to stress again is that the TMR monotonically increases with the increase of interface scattering potential, and therefore, the interface roughness emerging in the process of synthetizing the junction is not bad here.

Other parameters of the junction also may affect the TMR. The red dot-line in fig.5(a) shows the TMR's dependence on the thickness of ITB1, d_1, we can see that the TMR is almost unchanged with the variation of d_1. Although an increase of d_1 has small impact on the TMR, it can greatly suppress the magnetic proximity effect of FM2 to the TSC. Fig.5(b) shows

that the TMR has an oscillating dependence on the length of the FM2, d_2, this oscillating behavior is due to interference of wave functions in FM2. In fig.5(c), the TMR shows a dependence on M_1 which is similar to the inset of fig.1(d), where the TMR monotonically increases with the increase of the magnetization strength. The inset of fig.5(c) shows a remarkable property of the junction that even the FM1 turns to be a normal metal (NM), the TMR also grows exponentially with the increase of d_3. Therefore, a NM-I-FM-I-TSC junction is also an ideal structure for applications. In fig.5(d), it is shown that when the length of FM2 is large, *i.e.*, $k_{2+(-)}d_2 >> \pi$, TMR will exhibit an oscillating dependence on M_2, which is also due to interference of wave functions in FM2. However, when $k_{2+}d_2 < \pi$, TMR will exhibit a monotonically increasing dependence on M_2, as shown in the inset of fig.5(d). From fig.5(b)(d), we see that the interference of wave functions in FM2 may greatly suppressed the TMR, to avoid the suppression in real applications, therefore, the length of FM2 is better to choose to satisfy $k_{2+}d_2 < \pi$.

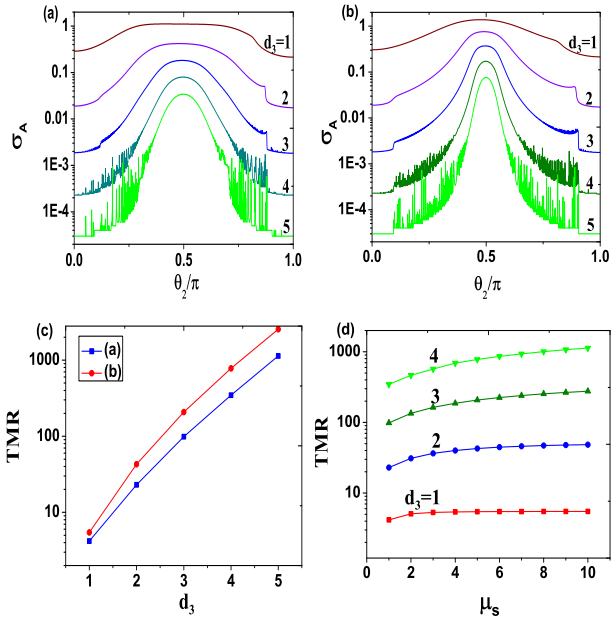

FIG. 6. Tunneling spectroscopy of FM-I-FM-I-TS junction in two dimension and TMR's dependence on parameters, logarithmic coordinates are used in all figures. Common parameters in all figures, $\mu_f = 1$, $\mu_I = 0.1$, $\Delta_0 = 0.05$, $M_1 = M_2 = 0.4$, $d_1 = 0.2$, $d_2 = 1$, $\theta_1 = \phi_1 = \phi_2 = 0$. Here choosing a small μ_I is to enhance the momentum filtering effect. (a)-(b) show the ZBC's dependence on θ_2 and d_3 with (a) $\mu_s = 1$, (b) $\mu_s = 5$. (c) shows the TMR-d_3 relation corresponding to (a) and (b). (d) shows the TMR-μ_s relation for different d_3.

V. HIGHER-DIMENSIONAL CASE

Here we only consider a two-dimensional FM-I-FM-I-TSC junction for illustration, the three-dimensional case can be directly generalized from it.

The two-dimensional Hamiltonian we consider under the representation $\hat{\Psi}^\dagger(\vec{r}) = (\hat{\psi}^\dagger_\uparrow(\vec{r}), \hat{\psi}_\downarrow(\vec{r}), \hat{\psi}^\dagger_\downarrow(\vec{r}), \hat{\psi}_\uparrow(\vec{r}))$ is given as

$$\mathcal{H}_{2D} = \tau_z \left[-\frac{\partial_x^2 + \partial_y^2}{2} - \mu(x) + V(x) \right] + \tau_x \Delta(x) + \tau_y \Delta(y),$$

here we have assumed that the chemical potential $\mu(\vec{r})$, the potential $V(\vec{r})$ and the pairing potential $\Delta(x)$ take the same form as $\mu(x)$, $V(x)$ and $\Delta(x)$ given previously, respectively. The other pairing potential $\Delta(y) = i\Delta_0 \Theta(x - x_1)\partial_y$.

When the dimension of the system is higher than one, the injected electron's momentum $\vec{k}$ can be decomposed as $(k_x, k_\perp)$, for the two-dimensional case we consider here, $k_\perp = k_y$. If $k_\perp$ is conserved in the process of electrons transporting across the junction, the tunneling process of an injected electron with nonzero $k_\perp$ at zero-bias voltage no longer exhibits the topological feature. This can be simply explained under the Majorana picture [51, 52]. In higher dimension, the boundary Majorana zero modes require $k_\perp = 0$, this indicates that due to the momentum conservation, an injected electron with nonzero $k_\perp$ will no longer directly couple with the Majorana zero modes, and then the ZBC will be parameter-dependent (topological feature is absent) no matter what value θ_2 takes. As the final conductance includes contributions from every direction, it is obvious that the new added dimension will generally mask the topological effect. However, as the conductance curve should be continuous, this implies that if the ratio of the transverse momentum to the longitudinal momentum in TSC decreases, the effect of the non-zero transverse momentum will decrease, and then the topological effect will be strengthened. One way to reduce the momentum ratio in TSC is to increase μ_s, since $k_{s,\perp} = k_\perp$ is independent of μ_s, while $|k_{s,x}|$ monotonically increases with μ_s.

The junction itself has an intrinsic effect to enhance the topological effect. The intrinsic effect is the so-called momentum filtering effect (MFE) [53] that is if $\mid \vec{k} \mid$ is fixed, then injected electrons with larger k_x will feel a lower tunneling barrier because the effective potential barrier is given as $U_{I,eff} = \mu_I + |\vec{k}|^2 - k_x^2 = \mu_I + |\vec{k}|^2 \sin^2\theta$ with $\theta = \arccos(k_x/|\vec{k}|)$. As the MFE reduces the contributions from injected electrons with larger $k_\perp$, the ratio of the contribution from the neighbourhood of $k_\perp = 0$ increases, consequently, the topological effect is also enhanced. Therefore, when the MFE is very strong, the TMR is expected to be very large. From the expression of $U_{I,eff}$, we know that the most direct way to enhance the MFE is to reduce μ_I, this can be realized by choosing small gap insulating materials as the ITB.

For the sake of discussion, we introduce a dimensionless quantity σ_A which is defined as

$$\sigma_A(\theta_2) = \frac{\sum_{k_y} \bar{G}(0, \theta_2, k_y)}{\sum_{k_y} 2e^2/h} \tag{20}$$

where $\bar{G}(0, \theta_2, k_y)$ is the summation of ZBC for spin-

up and spin-down electron with transverse momentum k_y. Fig.6(a)(b) shows that with the increase of d_3, ZBC will be greatly suppressed no matter what value θ_2 takes, this agrees with our previous argument. However, due to a combination of the topological effect and MFE, the suppression at the neighbourhood of $\theta_2 = \pi/2$ is still much smaller than the ones at the neighbourhood of $\theta_2 = 0$ or π. The angle-dependent suppression behavior results in an approximately exponential dependence between the TMR (now given as $(\sigma_{\mathrm{A,max}}-\sigma_{\mathrm{A,min}})/\sigma_{\mathrm{A,min}}$) and d_3, as shown in fig.6(c), therefore, the remarkable property of the FM-I-FM-I-TSC junction that the TMR is easy to tune and can be tuned to arbitrary high value is still hold in two-dimension. Compared fig.6(b) to fig.6(a), we can see that an increase of μ_s indeed results in an enhancement of the topological effect and consequently a slower decrease of σ_A at the neighbourhood of $\theta_2 = \pi/2$. Fig.6(c)(d) show that the slower decrease of σ_A results in a larger TMR. The effects of other parameters are similar to the ones shown in fig.5, we do not plan to discuss them here again.

VI. DISCUSSIONS AND CONCLUSIONS

In summary, because the tunneling process in junctions composed of FM and time-reversal invariant TSC without SRS strongly depends on the spin-polarization direction of the injected electrons, high TMR is found to exist in these junctions. Compared to conventional TMR shown in MTJs, the TMR shown in FM-I-TSC junction and FM-I-FM-I-TSC junction exhibits several extraordinary characteristics: (i) so far, the best mechanism to obtain high TMR in conventional MTJs is to take use of a MgO tunneling barrier [54–57], however, for junctions we have considered, high TMR is obtained even the ITB is featureless; (ii) for the FM-I-TSC junction in one dimension, the TMR only depends on the magnetization strength of the FM, and it goes to infinity when the FM turns to be a half metal; (iii) for the FM-I-FM-I-TSC junction, the TMR shows a remarkable property that it grows exponentially with the thickness of ITB between the two FMs and also grows monotonically with the interface scattering potential, this remarkable property makes it possible to tune the TMR to arbitrary high value even the magnetization strength of the two FMs are both weak, in fact, the magnetization strength of FM1 can even be zero. Even with a consideration of the effect of finite temperature, these characteristics will still hold if k_BT is much smaller than the energy gap of the TSC.

In short, a combination of the FM and TSC provides a new fascinating mechanism to obtain high TMR in a convenient way. Besides this remarkable effect, we also note there already exist some works pointing out that spin-polarized current, another important element for spintronics, can also be simply realized by making use of TSCs[50, 58]. All these results suggest that the nontrivial topological property of TSCs may bring new insights in spintronics.

VII. ACKNOWLEDGEMENTS

We thank Zhong Wang for useful discussions. This work is supported by NSFC under Grant No.11275180.

APPENDIX

When a spin-up electron with energy E is injected from the FM1, the wave functions in the two ferromagnetic parts are given as

$$\begin{aligned}\psi_{FM1} &= \vec{\chi}_1 e^{ik_{1+,e}x} + b_{1+}\vec{\chi}_1 e^{-ik_{1+,e}x} + a_{1+}\vec{\chi}_2 e^{ik_{1+,h}x} \\ &\quad + b_{1-}\vec{\chi}_3 e^{-ik_{1-,e}x} + a_{1-}\vec{\chi}_4 e^{ik_{1-,h}x}, \\ \psi_{FM2} &= b_{3L+}\vec{\chi}_1' e^{-ik_{2+,e}x} + b_{3R+}\vec{\chi}_1' e^{ik_{2+,e}x} + a_{3L+}\vec{\chi}_2' e^{-ik_{2+,h}x} \\ &\quad + a_{3R+}\vec{\chi}_2' e^{ik_{2+,h}x} + b_{3L-}\vec{\chi}_3' e^{-ik_{2-,e}x} + b_{3R-}\vec{\chi}_3' e^{ik_{2-,e}x} \\ &\quad + a_{3L-}\vec{\chi}_4' e^{-ik_{2-,h}x} + a_{3R-}\vec{\chi}_4' e^{ik_{2-,h}x},\end{aligned}$$

with $\vec{\chi}_1 = (\eta_1, 0, \eta_2 e^{i\phi_1}, 0)^T$, $\vec{\chi}_2 = (0, \eta_2, 0, \eta_1 e^{i\phi_1})^T$, $\vec{\chi}_3 = (-\eta_2, 0, \eta_1 e^{i\phi_1}, 0)^T$, $\vec{\chi}_4 = (0, -\eta_1, 0, \eta_2 e^{i\phi_1})^T$, where $\eta_1 = \cos(\theta_1/2)$, $\eta_2 = \sin(\theta_1/2)$; $\vec{\chi}_i' = \vec{\chi}_i(\theta_1, \phi_1 \to \theta_2, \phi_2)$; the momenta $k_{1,2+,e(h)} = \sqrt{2(\mu_f + M_{1,2} + (-)E)}$, $k_{1,2-,e(h)} = \sqrt{2(\mu_f - M_{1,2} + (-)E)}$. The wave functions in the two insulating parts are given as

$$\begin{aligned}\psi_{I1} &= b_{2L\uparrow}\vec{e}_1 e^{-k_{I,e}x} + b_{2R\uparrow}\vec{e}_1 e^{k_{I,e}x} + a_{2L\downarrow}\vec{e}_2 e^{-k_{I,h}x} \\ &\quad + a_{2R\downarrow}\vec{e}_2 e^{k_{I,h}x} + b_{2L\downarrow}\vec{e}_3 e^{-k_{I,e}x} + b_{2R\downarrow}\vec{e}_3 e^{k_{I,e}x} \\ &\quad + a_{2L\uparrow}\vec{e}_4 e^{-k_{I,h}x} + a_{2R\uparrow}\vec{e}_4 e^{k_{I,h}x}, \\ \psi_{I2} &= \psi_{I1}(b_{2\alpha\beta}, a_{2\alpha\beta} \to b_{4\alpha\beta}, a_{4\alpha\beta}), \alpha = R, L; \beta = \uparrow, \downarrow,\end{aligned}$$

where $\vec{e}_1 = (1,0,0,0)^T$, $\vec{e}_2 = (0,1,0,0)^T$, $\vec{e}_3 = (0,0,1,0)^T$, $\vec{e}_4 = (0,0,0,1)^T$, the momenta $k_{I,e(h)} = \sqrt{2(\mu_I - (+)E)}$. The wave functions in the superconducting part is given as

$$\begin{aligned}\psi_{TS} &= t_{5e}\vec{\lambda}_1 e^{ik_{s,e}x} + t_{5h}\vec{\lambda}_2 e^{ik_{s,h}x} + s_{5e}\vec{\lambda}_3 e^{ik_{s,e}x} \\ &\quad + s_{5h}\vec{\lambda}_4 e^{ik_{s,h}x}\end{aligned}$$

with $\vec{\lambda}_1 = (u_{1k}, v_{1k}, 0, 0)^T$, $\vec{\lambda}_2 = (u_{2k}, v_{2k}, 0, 0)^T$, $\vec{\lambda}_3 = (0, 0, u_{1k}, v_{1k})^T$, $\vec{\lambda}_4 = (0, 0, u_{2k}, v_{2k})^T$, where $u_{1(2),k} = \Delta_0 k_{s,e(h)}/N_{1(2)}$, $v_{1(2),k} = (E + \mu_s - k_{s,e(h)}^2/2)/N_{1(2)}$ with $N_{1(2)} = \sqrt{|u_{1(2),k}|^2 + |v_{1(2),k}|^2}$ the normalization coefficients. $k_{s,e(h)} = (-)\sqrt{Q_1 + Q_2} + i\sqrt{Q_1 - Q_2}$ with $Q_1 = (\mu_s - \Delta^2)$ and $Q_2 = \sqrt{\mu_s^2 - E^2}$ (when $E < \Delta\sqrt{2\mu_s - \Delta^2}$), or $k_{s,e(h)} = (-)\sqrt{2(Q_1 + Q_3)}$ with $Q_3 = \sqrt{E^2 + \Delta^4 - 2\mu_s\Delta^2}$ (when $E > \Delta\sqrt{2\mu_s - \Delta^2}$).

* yzhbo@mail.tsinghua.edu.cn

[1] B. D. Josephson, Phys. Lett. **1**, 251-253 (1962).
[2] M. Julliere, Phys. Lett. A **54**, 225-226 (1975).
[3] J. C. Slonczewski, Phys. Rev. B **39**, 6995 (1989).
[4] G. A. Prinz, Science **282**, 1660 (1998).
[5] S. S. P. Parkin et al, J. Appl. Phys. **85**, 5828 (1999).

[6] J. G. Zhu and C. Park, Mater. Today **9**, 36 (2006).
[7] C. Chappert, A. Fert and F. N. Van Dau, Nature Mater. **6**, 813 (2007).
[8] S. Ikeda et al, IEEE Trans. Electron Devices **54**, 991 (2007).
[9] A. Fert, Rev. Mod. Phys. **80**, 1517 (2008).
[10] X. L. Qi and S. C. Zhang, Rev. Mod. Phys. **83**, 1057 (2011).
[11] A. Yu. Kitaev, Physics-Uspekhi **44**, 131 (2001).
[12] S. R. Elliott and M. Franz, Rev. Mod. Phys. **87**, 137 (2015).
[13] A. Yu. Kitaev, Ann. Phys. **303**, 2 (2003).
[14] C. Nayak, S. H. Simon, A. Stern, M. Freedman and S. Das Sarma, Rev. Mod. Phys. **80**, 1083 (2008).
[15] L. Fu and C. L. Kane, Phys. Rev. Lett. **100**, 096407 (2008).
[16] Y. Tanaka, T. Yokoyama, and N. Nagaosa, Phys. Rev. Lett. **103**, 107002 (2009).
[17] J. D. Sau, R. M. Lutchyn, S. Tewari and S. Das Sarma, Phys. Rev. Lett. **104**, 040502 (2010).
[18] R. M. Lutchyn, J. D. Sau and S. Das Sarma, Phys. Rev. Lett. **105**, 077001 (2010).
[19] Y. Oreg, G. Refael and F. von Oppen, Phys. Rev. Lett. **105**, 177002 (2010).
[20] J. Alicea, Phys. Rev. B **81**, 125318 (2010).
[21] X. L. Qi, T. L. Hughes and S. C. Zhang, Phys. Rev. B **82**, 184516 (2010).
[22] A. C. Potter and P. A. Lee, Phys. Rev. Lett. **105**, 227003 (2010).
[23] T. D. Stanescu, R. M. Lutchyn and S. Das Sarma, Phys. Rev. B **84**, 144522 (2011).
[24] V. Mourik et al, Science **336**, 1003 (2012).
[25] A. Das et al, Nat. Phys. **8**, 887 (2012).
[26] M. T. Deng et al, Nano Lett. **12**, 6414 (2012).
[27] A. D. K. Finck, D. J. Van Harlingen, P. K. Mohseni, K. Jung, and X. Li, Phys. Rev. Lett. **110**, 126406 (2013).
[28] L. P. Rokhinson, X. Liu, and J. K. Fudyna, Nat. Phys. **8**, 795 (2012).
[29] S. Nadj-Perge et al, Science **346**, 602 (2014).
[30] S. Tewari, S. Das Sarma, C. Nayak, C. Zhang and P. Zoller, Phys. Rev. Lett. **98**, 010506 (2007).
[31] C. Zhang, S. Tewari, R. M. Lutchyn and S. Das Sarma, Phys. Rev. Lett. **101**, 160401 (2008).
[32] M. Sato, Y. Takahashi and S. Fujimoto, Phys. Rev. Lett. **103**, 020401 (2009).
[33] L. Jiang et al, Phys. Rev. Lett. **106**, 220402 (2011).
[34] S. Diehl, E. Rico, M. A. Baranov and P. Zoller, Nat. Phys. **7**, 971 (2011).
[35] Z. B. Yan, S. L. Wan and Z. Wang, Sci. Rep. **5**, 15927 (2015).
[36] A. P. Schnyder, S. Ryu, A. Furusaki and A. W. W. Ludwig, Phys. Rev. B **78**, 195125 (2008).
[37] A. Yu. Kitaev, AIP Conf. Proc. **1134**, 22-30 (2009).
[38] S. Ryu, A. P. Schnyder, A. Furusaki and A. W. W. Ludwig, New. J. Phys. **12**, 065010 (2010).
[39] C. L. M. Wong, and K. T. Law, Phys. Rev. B **86**, 184516 (2012).
[40] F. Zhang, C. L. Kane and E. J. Mele, Phys. Rev. Lett. **111**, 056402 (2013).
[41] M. Sato, Y. Tanaka, K. Yada, and T. Yokoyama, Phys. Rev. B **83**, 224511 (2011).
[42] Y. Tanaka, M. Sato, N. Nagaosa, J. Phys. Soc. Jpn. **81**, 011013 (2012).
[43] Z. B. Yan and S. L. Wan, Euro. Phys. Lett. **111**, 47002 (2015).
[44] Z. B. Yan and S. L. Wan, New. J. Phys. **16**, 093004(2014).
[45] B. A. Bernevig and T. L. Hughes, *Topological Insulators and Topological Superconductors*, Princeton University Press, (2013).
[46] G. E. Blonder, M. Tinkham and T. M. Klapwijk, Phys. Rev. B **25**, 4515 (1982).
[47] Y. Tanaka and S. Kashiwaya, Phys. Rev. Lett. **74**, 3451 (1995).
[48] S. Kashiwaya and Y. Tanaka, Rep. Prog. Phys. **63**, 1641 (2000).
[49] A. F. Andreev, Sov. Phys. JETP **19**, 1228 (1964).
[50] J. J. He, T. K. Ng, P. A. Lee, and K. T. Law, Phys. Rev. Lett. **112**, 037001 (2014)
[51] K. T. Law, P. A. Lee and T. K. Ng, Phys. Rev. Lett. **103**, 237001 (2009).
[52] K. Flensberg, Phys. Rev. B **82**, 180516(R) (2010).
[53] S. Yuasa et al, Euro. Phys. Lett. **52**, 344 (2000).
[54] W. H. Butler, X.-G. Zhang, T. C. Schulthess and J. M. MacLaren, Phys. Rev. B **63**, 054416 (2001).
[55] J. Mathon and A. Umerski, Phys. Rev. B **63**, 220403(R) (2001).
[56] S. S. P. Parkin et al, Nature Mater. **3**, 862 (2004).
[57] S. Yuasa et al, Nature Mater. **3**, 868 (2004).
[58] Y. Tanaka, T. Yokoyama, A. V. Balatsky, and N. Nagaosa, Phys. Rev. B **79**, 060505 (2009).